Delft University of Technology
Master of Science Thesis in Embedded Systems

# Spectrum-aware Passive Visible Light Communication

**Vivian Kristen Pascal Dsouza**


TU Delft Delft University of Technology

# Spectrum-aware Passive Visible Light Communication

Master of Science Thesis in Embedded Systems

Embedded and Networked Systems Group
Faculty of Electrical Engineering, Mathematics and Computer Science
Delft University of Technology
Mekelweg 4, 2628 CD Delft, The Netherlands

Vivian Kristen Pascal Dsouza

18 August 2022

**Author**
Vivian Kristen Pascal Dsouza
**Title**
Spectrum-aware Passive Visible Light Communication
**MSc Presentation Date**
25 August 2022

**Graduation Committee**

| | |
|---|---|
| dr. Marco Antonio Zúñiga Zamalloa | Delft University of Technology |
| dr. Ujwal Gadiraju | Delft University of Technology |
| Seyed Keyarash Ghiasi | Delft University of Technology |

The work presented in this thesis has lead to a paper which has been submitted to ACM SenSys 2022 for publication, pending review.

**Abstract**

The rapidly growing number of wireless devices typically use radio frequency for communication. However, in order to avoid using the expensive and increasingly congested radio bands, research areas are moving in the direction of using ambient light to form physical links in wireless communication systems. Unlike active Visible Light Communication (VLC) which controls the light source itself, passive VLC modulates the ambient light and results in low power transmitters as no energy is required for generation of the carrier wave. Similar to radio waves, visible light is also electromagnetic radiation and has wavelengths in the range of 400-700 nm. All previous work in passive VLC rely on switching the whole spectrum at the same time, and do not completely exploit using the full spectrum of light - reducing potential channel capacity.

In this thesis we propose a novel method to transmit and decode data, using liquid crystal cells that can modulate the spectrum. The main contribution of this thesis is to show that we can move from spectrum-agnostic to spectrum-aware modulation with passive VLC. The work in this thesis focuses on modulation and demodulation of such a communication link, and introduces novel methods of controlling the light spectrum. We build a prototype and demonstrate a multi-symbol communication link, and evaluate it with an effort to maximise the datarate.

*"It would appear that we have reached the limits of what it is possible to achieve with computer technology, although one should be careful with such statements, as they tend to sound pretty silly in 5 years."* – John von Neumann

# Preface

This thesis began as a side project to use machine learning for classification of spectrograms observed. Although inexperienced in communication systems, I was enticed by the open-ended challenges and promising initial results, and hence choose to pursue this subject for my thesis. From then, it has been a roller coaster adventure which has put my skills to the test at multiple disciplines including both hardware and software.

I am grateful to everyone who has helped me in this journey. First, I would like to thank my supervisors Marco and Keyarash for their continuous guidance. From them I have learnt to stay calm and begin over with a principled investigation when faced with unexpected results. I would also like to thank Koen Langendoen for his mentorship and valuable critique. Finally, I would like to thank my family and friends for always being by my side.

Vivian Kristen Pascal Dsouza

Delft, The Netherlands
18th August 2022

# Contents

# Chapter 1

# Introduction

Visible Light Communication (VLC), as the name suggests, uses visible light to form the physical link in a wireless communication system. Light producing devices are ubiquitous in present-day society and they can easily be adapted to transmit information. Most wireless devices today use Radio Frequency (RF) for communication. However, as the radio frequency spectrum is getting increasingly crowded and expensive, new methods for communication are required to ease congestion. Not only does visible light escape this crowded spectrum, but it also introduces a vast bandwidth of about 400 THz. A key advantage of using the visible light spectrum apart from this increased bandwidth is that it has enhanced security. As visible light does not penetrate opaque surfaces with which most modern spaces are built, it is significantly less prone to sniffing attacks prevalent in radio communications.

Recently, research has been moving in the direction of Passive VLC which uses ambient light like sunlight or artificial indoor lighting to form the carrier wave. First introduced as back-scattering systems, these devices typically modulate the ambient light by using Liquid Crystal (LC) shutters [34] or MEMS mirrors [36]. Most approaches use LC shutters to control the amount of ambient light passing through them as a method of transmitting information. As the liquid crystals consume less than a mW of power, they save several watts of power when compared to active systems that use an illumination source. Thus, passive VLC is extremely energy efficient and forms a sustainable communication technology for future generations where it is expected to have many more smart wireless devices. Due to the low power transmitters of passive VLC, it is also better suited to applications with limited power availability and systems using energy harvesting.

Previous work employing such Passive VLC systems use the LCs to either block or allow the light through using on-off keying (OOK) [21] , or amplitude modulation schemes [33]. Like radio waves, visible light is also electromagnetic radiation with wavelengths in the 375-800nm range. The spectrum of a phone's flashlight can be seen in Figure 1.1 and shows the intensity of light at various wavelengths.

However, while the radio communication systems use sub-band modulation, passive VLC systems until now have been agnostic of the light spectrum and considered all ambient light as equal by integrating them into only few parameters. Hence, the resulting modulation schemes are either amplitude based

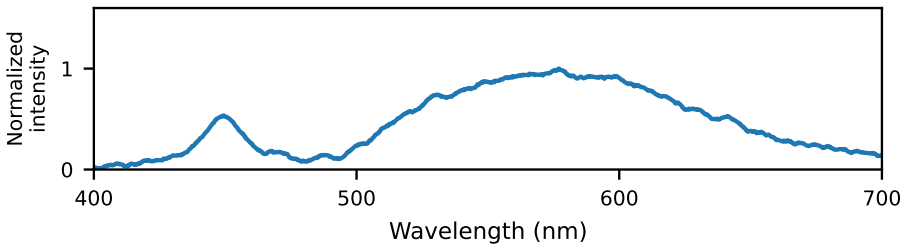


Figure 1.1: **The Spectrum of a phone's flashlight with the intensity at different wavelengths**

[34, 7, 32] or time-dependent [33]. These methods use a photo-diode, which measures light intensity across all wavelengths, or a camera or color sensor which distinguishes the RGB values to produce 3 parameters. Thus, these previous works discard the information coming from the individual wavelengths. It is also worth noting the human eyes perceive the full visible light spectrum in only 3 dimensions of RGB. Hence, just like our own eyes, cameras and color sensors too do not fully exploit the full spectrum's potential for information transfer.

Unlike these spectrum agnostic methods, using a spectrometer that measures the intensity of light at finer wavelength bands provides us with a much richer insight, allowing for more bandwidth.

The fundamental difference between radio communication and passive VLC is that while bandpass filters with high Q-factors enable transmitting and receiving to individual sub-bands in radio communications, such filtering is not easily possible with liquid crystals. Although optical filters can selectively transmit particular wavelengths of light - they do not possess sharp filter responses and cannot be easily combined with LCs without creating a complex and bulky setup.

Instead, recent work by Ghiasi et al. has shown that instead of only switching between purely opaque and purely translucent states, LCs have a rich transition space too [14]. This transition space could be used to create modulation schemes that go beyond the single parameter of light intensity. The voltage driven LCs manipulate the spectrum of the light passing through them.

Hence, by controlling the voltage applied on the LCs, we can modify the spectrum of light at the transmitter and use a spectrometer to recognize the information of the full spectrum at the receiver. This allows us to exploit potential bandwidth that was previously untapped.

Based on this, the contributions of this thesis are:

1. *A novel modulation-demodulation method that shows how our theoretical model can be used with off-the-shelf LCs.*We select symbols in the spectrum domain to transmit data. We will show that the received signals resemble spectrograms, and we decode packets using machine learning algorithms.

2. *We evaluate our proposed schemes by testing it on a prototype under different setups.* We build a transmitter based on LC cells, and we use a spectrometer in the receiver. To show the effect of different light spec-

trum, we test our link using different light sources, and we compare the performance and bit error rates (BER) of the system in various scenarios.

This brings us to define the concrete research goals of this thesis.

## 1.1 Problem statement

The fundamental objective of this thesis is the following:

| To establish the working of spectrum-aware passive visible light communication and maximize the datarate of the communication link. |
|---|

Given the hardware already set up, the problem statement can be broken into three broad yet concrete research tasks:

1. To investigate the dynamic behavior of the LC spectrum, and propose a suitable modulation scheme considering the underlying physics.
2. To analyze the spectrograms observed at the receiver and propose a suitable demodulation scheme to identify the symbols transmitted.
3. To evaluate the communication link in various conditions and maximize the datarate while keeping the Bit Error Rate (BER) within acceptable limits (below 1%).

These broader research goals each present their own challenges and will be discussed in the following chapters. Next, we take a look at the outline of this thesis.

## 1.2 Structure of the thesis

In Chapter 2 we take a look at the state of the art to understand the previous work in the field and attempt to make a fair comparison. Next, in Chapter 3 the key idea of this thesis and the use of LCs in passive VLC communication is explained. We begin our study by investigating the behavior of LCs and presenting a feasible modulation scheme in Chapter 4. In the following Chapter 5 we present the demodulation challenges and propose novel methods to identify the symbols transmitted and their location. In Chapter 6 we evaluate our communication link in various scenarios such as varying distance and measure the BER and overheads. Finally, we summarise the findings in Chapter 7 and explore possible avenues for future work in Chapter 8.

# Chapter 2

# Related work

Passive VLC is being actively researched for about the past eight years and has made significant progress. It finds applications not only in communication systems like our own, but also in localization, especially for indoor systems, and activity recognition [17]. In this chapter we summarise the previous work done in the field to provide the necessary background and allows us to make a fair comparison to evaluate our system later on.

In our work, we introduce for the first time the spectrometer as the receiver. This presents us with many new challenges which require an additional in-depth study to analyze spectrograms at the receiver. Thus, our background studies need to cover multiple disciplines. We start with the state of art in passive VLC, and then proceed to explore options for signal processing and classification methods to identify the symbols which we will use in the demodulation steps.

## 2.1 Prior work in communication systems

To analyze the state-of-the-art systems in communication we focus on prior work that use liquid crystals for passive VLC. We separate previous work into reflective and transmissive based on their use of the light source. Back-scattering (reflective) methods *typically* use an artificial light source and modulate the reflected light to form the up-link of the communication system. Transmissive systems on the other hand use any ambient light source and modulate the incident light directly.

### 2.1.1 Reflective

Back-scattering methods like Retro VLC [21] use active VLC to form the down-link part of the communication system. As the receiver is a low-power tag and cannot afford any high power consumption communication systems, they employ passive VLC by reflecting back the source light. This is done by using a combination of a LC cell and a retro-reflector. A retro-reflector is a device that reflects any incident light back in the direction of the source. Pixelated VLC-Backscattering uses almost the same methods as Retro VLC [25] except that they use a grid of multiple LCs to create more complex modulation schemes to increase channel capacity. It is worth noting that these methods still rely on

the intensity of light modulated and not the spectrum. They achieve datarates of 500 - 600 bps.

An improvement of RetroVLC - PassiveVLC uses a similar platform as RetroVLC, but improves the modulation scheme [34]. While RetroVLC uses manchester encoding, PassiveVLC uses the more efficient Miller encoding. The bottleneck in using LCs in communication is that they have a slow discharging phase. The LCs switch quickly when a voltage is applied because of the energy supplied by the electrical fields. However, on discharging they only have their own intermolecular force to return to their original position which requires significantly more time. As the miller encoding sends fewer transitions - fewer switches are required, and thus it is able to speed up communication and achieves a datarate of 1 kbps at a distance of 1 meter.

RetroI2V is designed for infrastructure to vehicle communication using passive VLC [32]. They attempt to communicate between a vehicle and signage alongside the roads by using the vehicle's headlights itself for an active VLC down-link. The signage use retro reflectors to send back additional information to the vehicle. Like PassiveVLC , RetroI2V also uses the more efficient miller encoding. However, the signage uses larger surfaces (36x) and more powerful lamps (10x) along with two photodiodes to reduce the BER. They are able to achieve a similar datarate of 1 kbps as PassiveVLC, but push the distance to ranges of 1 meter to 80 meters.

RetroTurbo uses multiple LCs, along with four photodiodes which use two different polarizers placed at 45 degrees to each other [33]. This creates two independent channels for the communication link to use. They also propose a new modulation scheme called Delayed Superimposition Modulation (DSM) which takes advantage of the faster charging phase of the LCs. They introduce Polarized QAM which uses a constellation with 16 symbols. This requires an array of 64 LCs at the transmitter. With this hardware, they are able to achieve a remarkable datarate of 8kbps at a distance of 7.5 meters.

### 2.1.2 Transmissive

Similar to the platform we use, transmissive systems let the ambient light pass through them directly. However, unlike our platform which uses a spectrometer as a receiver, they use photodiodes or color sensors.

Unlike the works presented until now, LuxLink uses Frequency based modulation instead of amplitude based modulation [7]. It uses an LC along with a diffuser to modulate the ambient sunlight by modulating the frequency of the transmitted signal. At the receiver, a Fourier transform is used to demodulate the signal. This frequency-shift-keying has the main advantage of being intensity independent, and is ideal for varying intensity sources like sunlight. However, they still use only the extreme states of the LCs without using the intermediate transition voltages. They achieve a datarate of 80bps at a range of 65 meters with this novel approach.

The systems until now did not make use of color based modulation schemes. PIXEL uses LCs to generate colors for Visible Light Positioning (VLP) systems. They achieve a datarate of 14 bps which is sufficient for positioning systems, and can be increased by increasing the sampling rate of the camera [35]. Similarly, POLI presents a long range light-to-camera communication system [8]. They

| Passive Visible Light Communication | | | | |
|---|---|---|---|---|
| **Name** | **Data rate** | **Range** | **LC count** | **Receiver** |
| RetroVLC | 0.5 kbps | 2.4 m | 1 | Photodiode |
| PassiveVLC | 1 kbps | 1 m | 1 | Photodiode |
| RetroTurbo | 8 kbps | 10 m | 64 | Photodiode |
| POLI | 71 bps | 40 m | 1 | Camera |
| PIXEL | 14 bps | 10 m | 1 | Camera |
| Luxlink | 80 bps | 4.5 to 65 m | 1 | Photodiode |
| ChromaLux | 1 kbps | 1 to 50 m | 4 to 6 stacked | Colorsensor |

Table 2.1: **Comparison with state-of-the-art.**

make the system flicker-free, so that it is insensitive to the human eyes by using polarized light. It achieves a datarate of 71bps at a distance of 40 meters.

Chromalux is similar to our own platform by virtue of stacking multiple LCs together at the transmitter [14]. They use 6 LCs and introduce the insight of using intermediate voltages to various colors. This transient state allows them to speed up transmission with more complex constellations. Using sunlight they achieve a datarate of 1kbps at an impressive distance of 50 meters.

Other studies such as PolarTag create patterns to transmit static data similar to QR codes [27]. Some works such as [28] use tags along with polarized light to help IMU's in indoor localization tasks. Both of these studies take advantage of the fact that the human eyes are insensitive to polarised light and hence avoid potentially harmful flicker.

No prior work in passive VLC uses a spectrometer to exploit the full potential of the visible light spectrum. A summary of all related work is presented in Table 2.1.

## 2.2 Prior work for novel demodulation scheme

The spectrogram produced by the receiver in our platform is a graph that portrays the change of intensities at each wavelength in the spectrum with time. To be able to identify the symbols from the spectrogram and classify them, we take a look at previous works using spectrograms.

Spectrograms find a lot of applications when used with audio. They are used for speech recognition in applications like dictation and telephony [20]. These methods use the visualization of the spectrogram to find particular patterns. For example, popular music recognition software Shazam, uses a fingerprint of constellations to index millions of songs and identify them quickly with only a short snippet [31]. Multiple works such as [37] use spectrograms to identify the phonetic information of speech. From these works, we conclude that a visual representation of the spectrogram as an image can be used to infer information from the audio in the frequency domain. We can use a similar approach with the visible light spectrum.

In comparison to audio, the spectrum of visible light is not as extensively explored. Many studies focus on the spectrum of artificial LED lighting for comfort and aesthetics. Vanderveen et. al. develop an inexpensive light spectrometer for chemical engineering applications like determining the absorbance

of dyes [29]. The study of the spectrum of light is also used in Field Spectroscopy where the reflectance of natural solar illumination is measured at all wavelengths to characterize the vegetation, soil and rocks. Some studies use the visible light spectrum for molecular detection. For example, spherical gold nanoparticles can be identified by the visible light spectrum they reflect [22]. However, these studies only rely on a static measurement and do not consider the change in the spectrum with time.

As far as we know, no other studies use spectrograms in visible light communication systems. In our case, we require to identify the location of the symbols in the spectrogram and classify them. Fortunately, spectrograms can be represented as a 2-dimensional image, with each pixel represented by a number denoting the intensity of light at a particular wavelength. There has been plenty of progress made in the field of digital image processing over the past century which we can make use of. Multiple techniques in image processing are suitable for extracting edges and features from images to obtain information [5]. Not only that, but identifying and classifying objects in images too has been in focus with the rise in machine learning methods [18].

Methods in deep learning too can be used for classifying images [15]. However, they typically employ complex models which require large data sets and long training time. Thus, they are not preferable for our communication link which will be deployed in an embedded application in the final solution. Still, hardware for deep learning models in small IoT applications is becoming increasingly available and popular [30]. Hence, while not preferable, we do not completely rule out the use of deep learning for demodulation.

# Chapter 3

# Spectrum Aware Passive VLC

In this chapter, we first take a look at what LCs are and explain their working. Then we describe the general concept of this thesis about using the full spectrum in Passive VLC. Next, we explain the platforms used for the transmitter and receiver in the experiments of this thesis. To be able to achieve deterministic operation of the LCs in our communication link we analyze the spectrum they output at different applied voltages. We also take a look into the effect of stacking multiple LCs together, which produces a richer spectrum [14].

## 3.1 Working of LC cells

In order to understand the working of LCs in passive VLC, we must first understand what LC cells are and their basic functionality. LCs are transparent crystals that can change the polarization angle of the incident light passing through them. The polarization angle is the geometrical orientation of the oscillations of the electromagnetic waves of the light. The oscillations are perpendicular to the direction of motion of the wave, like shown in Figure 3.1. The orientation of the crystals in the LCs change the polarisation angle of the incoming light.

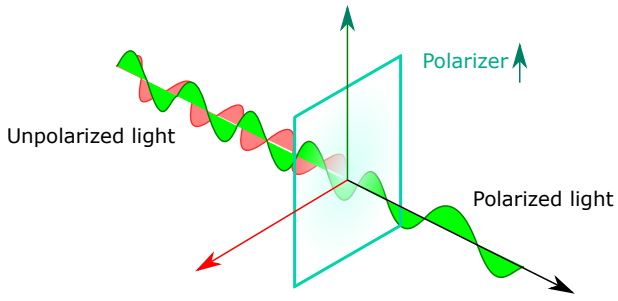


Figure 3.1: **Polarization of light using a polarizer. Only the waves oscillating with certain polarization angles can pass through, like the green wave in this example.**

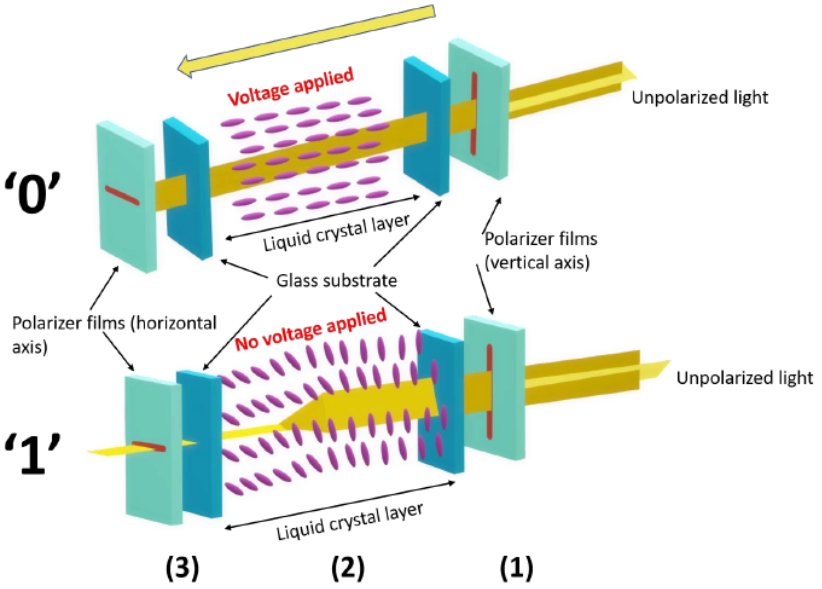


Figure 3.2: **Working of LC shutters** [7]

The interesting and important feature of LCs is that the applied electrical field decides the rotation angle of the light exiting the crystal. Changing the applied voltage on the LC will subsequently change the polarisation angle of the exiting light.

LC shutters exploit this phenomena by sandwiching the crystals between two sheets called a polarizer and analyzer. Most ambient light is unpolarised, meaning the constituent waves oscillate in all directions, as can be seen before the light enters the polarizer in Figure 3.1. The polarizer restricts the polarization angle of the incoming light to a single vertical angle, seen in layer 1 of Figure 3.2. Thus only the waves oscillating in that particular orientation are allowed to pass through. The second sheet - the analyzer, is placed after the LC material as can be seen in layer 3. Like the polarizer, it too ensures that only the light waves with a particular polarization angle may pass through. The polarization angle of the LC material is such that when there is no applied voltage on the LCs, the light will be rotated to pass through the analyzer thus making the LC shutter appear transparent. This is determined by the thickness of the LC. However, when a voltage is applied to the LC material the light is rotated and can no longer pass through the analyzer, making the shutter appear opaque.

In this way, Liquid Crystals are commonly used to block or allow light to pass through. Due to the application of these LCs in displays and optical shutters, most off-the-shelf LCs are designed for either completely blocking or allowing all light to pass, and are rated for use with applications requiring these binary states of operation. Only recently, Ghiasi et al. [14] have shown that by applying the intermediate voltages, interesting colors can also be achieved with these LC shutters. The colors are produced due to the effect of birefringence, which we will explain in subsection 3.4.1. While these colors were used to increase the

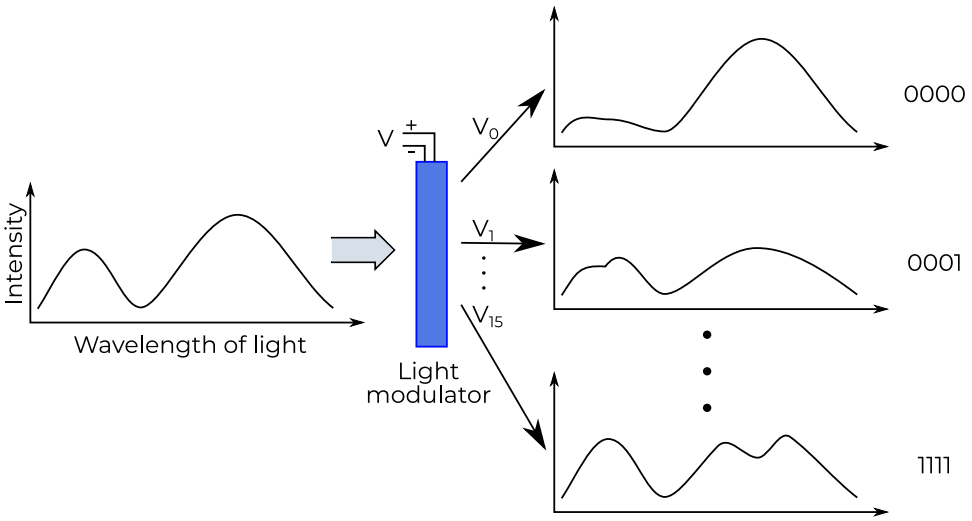


Figure 3.3: **General idea of the thesis**

datarate in OOK modulation in their work, we conjecture that they can also be used to produce a diverse array of spectrum observed with the spectrometer to create a multi-symbol communication link. We explain the general idea in the following Section 3.2

## 3.2 General concept

The spectrum of light can be modulated with a LC cell by changing the applied voltage, and can be used to create a multi-symbol communication link. The changes in the spectrum can be observed by a spectrometer, which measures the intensity of light at individual wavelength bands as shown in Figure 1.1. By selecting voltages that will produce a unique spectrum observed at the receiver, we can create a *communication symbol*. By changing the applied voltage we can send different symbols to increase the datarate of the system. This idea is illustrated in Figure 3.3.

To be able to use the light modulator in this way, we must understand the relationship between the applied voltage and the spectrum of light exiting the LCs. Next, we will understand the optics of Liquid crystal shutters and see how the thickness of the LC cells affects the spectrum. After that, we look at how the spectrum of light passing through responds to the voltage applied. This understanding will allow us to choose optimal symbols for our communication link later.

## 3.3 Platforms

Before we begin addressing the challenges of the operation of our communication link, we take a brief look at the physical setup we use. We first explain the transmitter which uses the LCs, before moving on to the receiver which uses the spectrometer.

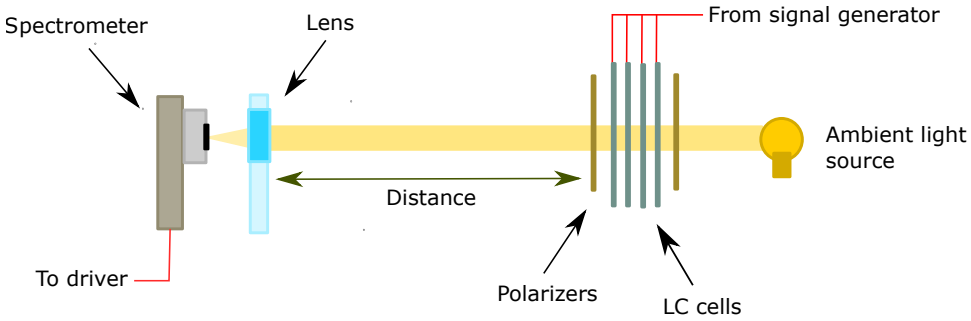


Figure 3.4: **Experimental setup**

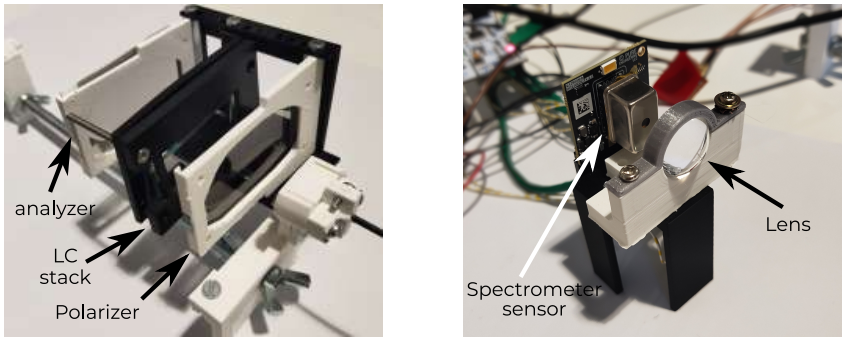


(a) Transmitter with LC stack

(b) Receiver with Spectrometer

Figure 3.5: **Images of the transmitter and receiver**

### 3.3.1 Transmitter

The transmitter uses a stack of 4 LCs which modulate the ambient light. We stack multiple LCs to enhance the optical response which will be explained in subsection 3.4.2. These LCs are modulated in parallel by a voltage supply ranging from 0 V to 20 V. This voltage is supplied to the LCs by a signal generator which creates the required waveforms for modulation. Although the LCs themselves can tolerate much higher voltages (about 100V) , we are unable to operate at those ranges due to the limitation of our signal generator's maximum output voltage. We leave this point for consideration while discussing future work in chapter 8.

The experimental setup is illustrated in Figure 3.4. First, the unpolarised ambient light enters the polarizer and is modulated by the stack of four pi-cells. The light exits through the analyzer and is directed towards the receiver. We experiment with different kinds of light sources: a phone's flashlight, standard room light bulbs, a sunlight emulator and real sunlight. In the case of the phone's flashlight, an optical cable is used from the light source and directed through a lens onto the polarizer.

### 3.3.2 Receiver

The receiver of our system is a C12880 Hammamatsu Spectrometer chip. We choose this spectrometer as it is able to obtain the intensities of the spectrum with sufficient precision, and has the ability to sample at at least twice the communication link's speed to satisfy the Nyquist criteria. The spectrometer is a 1-D CMOS linear image sensor array with each pixel exposed to a particular band of wavelengths only. The spectrometer is sensitive to wavelengths of light between 340nm to 850nm. It has a dedicated driver PCB, which generates the clock pulses and converts the analog output of the spectrometer to digital for the PC to read. We use a lens to focus the light coming from the transmitter onto the sensor of the spectrometer. All the video data from the spectrometer is transferred to a PC which in turn performs the next steps of demodulation. At this point, our goal is to establish the proof-of-concept of spectrum-aware passive VLC, and we do not perform real time demodulation. All the decoding is performed offline on the PC which runs the classification algorithms.

An image of both the transmitter and receiver can be seen in Figure 3.5. The costs of the platforms and power consumption can be found in Appendix A.

## 3.4 Characteristics of LC cells

### 3.4.1 Optical properties

We first explain each of the parameters which affect the optical properties of the LC cells. The optics of an LC cell are primarily defined by three factors that decide the intensity of light passing through, and the color shift. These are:

1. The material's birefringence
2. Thickness of the LC
3. The wavelength of the light passing through

When light passes through transparent materials it travels at a reduced speed when compared to traveling through free space. The ratio of these two speeds is called the refractive index of the material, and is given by:

$$n = \frac{c}{v}, \tag{3.1}$$

where $c$ is the speed of light in free space, and $v$ is the speed of light through the material. In materials exhibiting birefringence, such as crystals, the light passing through breaks into two perpendicular components, each creating its own refractive index. This can be seen in Figure 3.6 with the red wave (A) being split into orthogonal components green (B) and yellow (C) with varying speeds due to the different values of $n$. Birefringence is defined by:

$$\Delta n = n_l - n_h, \tag{3.2}$$

where $n_l$ and $n_h$ are the refractive index of the lowest and highest speed respectively. Materials exhibiting birefringence have a polarization-dependent refractive index, given by:

$$n = \frac{n_l}{n_h} \tag{3.3}$$

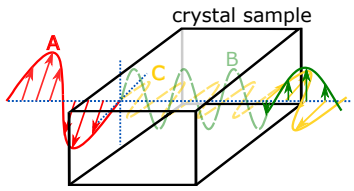


(a) Crystal exhibiting birefringence with light spilt into two orthogonal components with different speed

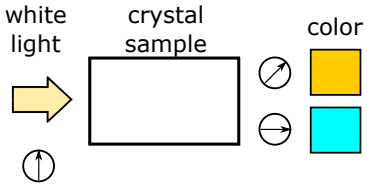


(b) White light passing through a crystal outputs colors based on birefringence when viewed through an analyzer

Figure 3.6: **Birefringence in crystals creating different colors [14]**

When the polarised light enters birefringent material, a phase shift between the two waves is observed, leading to circular polarization upon exiting the material [26]. The *path difference* ($\Gamma$) is dependent on the material's birefringence and thickness, and is defined as:

$$\Gamma = \Delta n \cdot d \tag{3.4}$$

where $d$ is the thickness of a crystal, and $\Delta n$ its birefringence.

The path difference ($\Gamma$) and the wavelength of light ($\lambda$) passing through, impact the intensity of light passing through the crystal. As explained in Section 3.1, only the light with a rotational angle aligned with the analyzer's polarisation angle will pass through, with all other orientations being filtered out (seen in layer 3 of Figure 3.2).

According to [19], when the polarizer is perpendicular to the analyzer, this effect is captured by the following equation:

$$L(\Gamma, \lambda) = sin^2(\frac{\pi\Gamma}{\lambda}) \tag{3.5}$$

where light intensity $L$ is defined as the ratio between the intensity of a wavelength after the analyzer, and before its entrance to the crystal.

To understand the effect of Equation 3.5 on the spectrum of an ambient light source, we should consider the amplitude of the various wavelengths in the emitted spectrum of the light. The amplitude $A_o$ of the light ray at the output of the analyzer is computed as follows:

$$A_o(\Gamma, \lambda) = A_i(\lambda) \times L(\Gamma, \lambda) \tag{3.6}$$

where $A_i$ is the amplitude of the input light for wavelength $\lambda$, $\Gamma$ the path difference of the LC cell. The final color of the light outputting from the LC cell is decided by all the amplitudes of the individual wavelengths.

### 3.4.2 Stacking LCs

Now that we have a basic understanding of LC optics with (3.4)-(3.6), we can assess the theoretical impact of path difference on the spectrum. Changing the applied voltage affects the birefringence, which can be used to change the path difference as shown in (3.4). The impact of path difference on the spectrum can

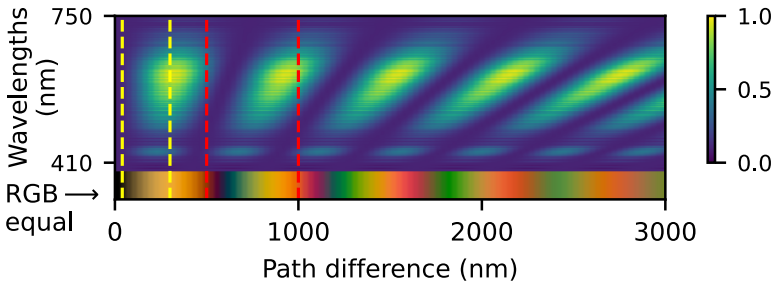


Figure 3.7: **Modeled impact of path difference on flashlight spectrum per wavelength. The bottom color shows the combined effect of the wavelengths in the above column.**

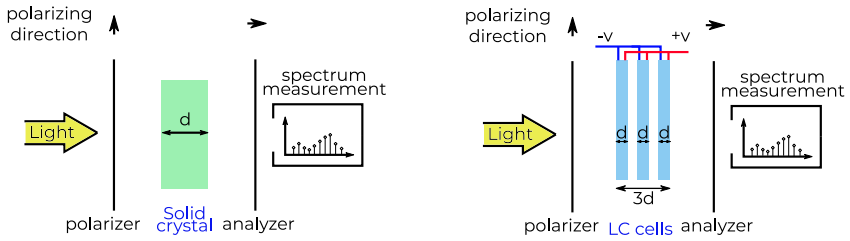


(a) Using a solid crystal

(b) Using multiple LCs

Figure 3.8: **Stacking LC cells as an alternative to thick cells to attain increased path difference**

be seen in Figure 3.7, where $\Gamma$ is increasing from 0 to 3000 nm. The colors are representative of the intensity at that particular wavelength with yellow being the highest and dark blue the lowest at zero intensity. The intensity at different wavelengths is measured, and the corresponding color is derived from the CIE 1931 color space.

We use this insight to be able to choose symbols in our communication link that differ from each other so that they may be easily classified at the receiver. However, our choice is limited as most off-the-shelf LC cells are designed to operate between the $\Gamma = 0$ and $\Gamma = 70$, marked with the yellow dashed lines. It is apparent from the modeling that richer and more diverse spectra exist for larger path differences, which can be created by thicker crystals. As we saw in (3.4) the path difference is directly proportional to the thickness of the liquid crystal.

Since crystals with these larger thickness values are not readily available commercially, we approximate its effect by stacking multiple thinner crystals together - to modify the path difference. This idea is illustrated in Figure 3.8. It is worth noting that this idea is not perfect, as the liquid crystal material is sandwiched between two glass electrodes. Stacking the LCs results in a number of glass electrodes in between the liquid crystal material which attenuates the signal.

In order to best recreate the effect of the single solid LC, all the LCs in the

stack are modulated together by the same applied voltage. This is because modulating with each LC independently (i.e with different applied voltages to each cell) leads to worse results, as it affects the homogeneity of the crystal behaviour.

## 3.5 Relation between voltage and spectrum

In all prior works pertaining to passive VLC, the receiver has mostly been a photodiode. The photodiode measures the intensity of light integrated over a broad range of wavelengths. Hence LCs have so far been used in such systems by switching between the extremes of completely opaque and translucent. However, we propose using a spectrometer as a receiver, which is able to give us a much deeper insight into the LC states. We saw in subsection 3.4.1 how different colors can be transmitted by changing the path difference, which is controlled by the voltage on the LCs. The different colors of light passing through the LCs affect the intensities at different wavelengths which can be identified by the spectrometer.

Now that we understand the optical properties of LCs, we need to understand how the spectrum responds to voltage applied on the LC stack. We perform two kinds of analysis in this thesis:

1. Static analysis - To determine the optical behavior of the spectrum at various voltage levels - assuming a long time window for the crystal to settle down after each change.

2. Dynamic analysis - To measure the settling time of the optical spectrum when switched between different voltage regions. This will be explained further in chapter 4

The static analysis will help us choose voltages that result in spectra that are distinguishable from each other. In this analysis, we do not take into consideration the time-dependant behavior of the LCs and only take a look at the spectrum after they have settled at their final state (after 1 s).

Figure 3.7 shows us that a broader covered range of path difference will result in more diverse spectra. In order to increase the range of the path difference, the thickness of the liquid crystal must be increased, or alternatively (in our case) more LCs must be stacked. However, we must consider the trade-off between increased path difference (and resulting richer spectra) vs the attenuation of light passing through. This attenuation of the signal will limit us in increasing the distance between the transmitter and receiver in our communication link. Not only that, but as the thickness of the cell increases (or more cells stacked), the path difference increases, and the colors begin to fade as shown in the Michel-levy chart in Chromalux [14]. Hence, we use the minimum number of LCs that produce a sufficiently diverse spectrum.

There are a few choices for LC shutters available off-the-shelf. Most LC shutters work on the twisted nematic field effect which align the molecules by the application of an electrical field. The molecules in the liquid crystal material, shown in pink in Figure 3.2, change the polarization angle of the incident light such that outgoing light will either pass through or be blocked by the analyzer. Introduced in 1984, pi-cells are LC shutters that also use the twisted nematic

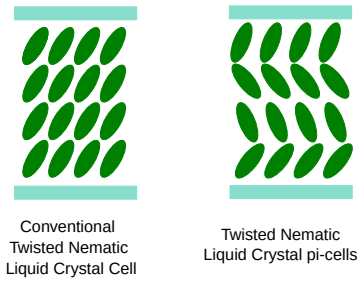


Figure 3.9: **Comparison of molecular alignment of conventional TN cells vs pi-cells**

effect, but have faster switching cycles due to the fluid dynamics and alignment of the molecules. A schematic of the molecular arrangement is shown in Figure 3.9. The conventional cells have a uniform alignment of molecules while the pi-cells have a 180 degree twist in the molecules between the electrodes. For conventional TN cells, when the electric field is switched off, the molecules in the mid-layers feel a torque, which causes a back-flow within the fluid layers as they try to return to their original state. This resistance offered by the back-flow does not occur in the case of pi-cells, making them faster [2].

In our system, we make use of these faster pi-cells manufactured by Liquid Crystal Technologies [1]. In order to choose the optimum number of LCs to stack together, we require the $\Gamma$ values of these LCs, along with their relationship with voltage. However, like most manufacturers, these details are held back as propriety information and not provided when the LCs are purchased off-the-shelf. Hence, we resort to making empirical measurements to determine the corresponding spectrum characteristics with the increasing number of LCs.

In order to do this, we stack the LCs as shown in the right side image of Figure 3.8, and sweep the voltage applied on the stack from 0 volts to 20 volts. The idea of stacking LCs is inspired by Chromalux [14], but we make two improvements - the use of faster pi-cells and a higher number of symbols.

The experimental setup used for measuring the characteristics is shown in Figure 3.4, with the signal generator used to change the voltage on the LC cells for modulation. The flashlight of a phone was used as an ambient light source. The distance between the polarizer and lens was 20cm. The characteristics of the spectrum observed with 1, 2 and 4 LCs stacked together can be seen in Figure 3.10. These graphs show the intensity of light at each wavelength band, when the voltage is swept from 0 V to 20 V in steps of 100 mV. Each measurement was taken 1 second after the voltage was switched, which allows plenty of time for the LC optics to settle ensuring stable results. This does not account for the dynamic behavior of the LCs which we will look into later.

It is apparent from Figure 3.10 that increasing the number of LCs results in more patterns seen in the spectrum. The more distinctive patterns are preferable because they are easier to distinguish at the receiver end. Most importantly, we can conclude from these graphs that the spectrum of light passing through the LCs can be modified by changing the applied voltage. For the rest of this thesis we will work with 4 LCs stacked together as they produce a more diverse spectra for reasons explained above.

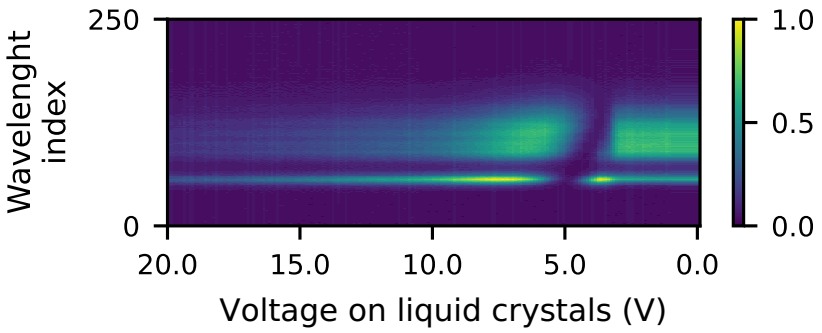


(a) 1 LC

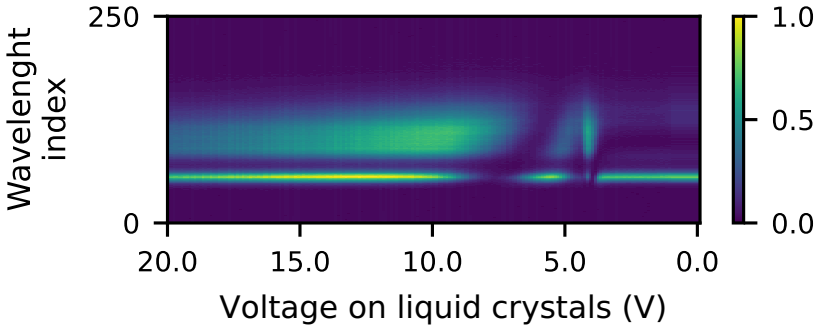


(b) 2 LCs

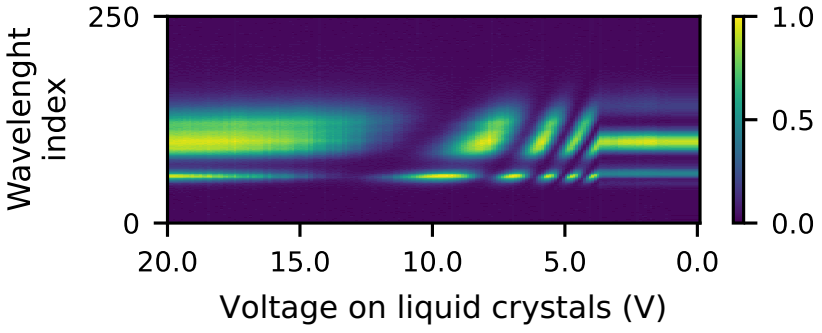


(c) 4 LCs

Figure 3.10: **Spectrum observed for different voltages using 1, 2 and 4 LCs stacked together**

# Chapter 4

# Modulation

So far, we have seen how the light spectrum can be modified by changing the voltage on LC cells. As the spectrum varies continuously across the voltage range, we can select multiple voltage levels - each with its unique spectrum signature, to transmit information. This creates a *multi-symbol* communication link, with each selected voltage level corresponding to a symbol. In this way, each symbol is encoding a string of bits, identifiable from its spectrum signature.

In radio communications, switching between any two symbols requires the same amount of time. However, when using LCs for modulation, we find that there is a dissimilar switching time for different voltage pairs. Thus, modulation is more complex than simply choosing the optimal symbols by selecting the most distinguishable spectrum signatures from the static spectrum behavior seen in Figure 3.10. The timing has to be considered as well. This is because waiting for long periods of time for the optical transition to stabilize is not feasible in a communication link - as it will dramatically reduce the datarate. On the other hand, using a switching frequency higher than the actual time required to switch will cause inter-symbol interference.

In this section, first we investigate the *dynamic* behavior of the LC spectrum to avoid the explained issues above, and then, we propose a suitable modulation scheme considering the underlying physics.

## 4.1 Settling time

When the voltage on the LCs is switched - the optical transitions seen in the spectrogram behave similar to a capacitor's exponential charging and discharging curves. The settling time is defined as the time required to complete an optical transition when the voltage applied on the cells is switched from a start voltage ($V_s$) to an end voltage ($V_e$). Some prior studies have evaluated the dynamic behavior of pi-cells from a material science perspective. In [9], the dynamic behavior of pi-cells is modeled using hydrodynamic equations of Ericksen-Leslie, and simulated. A large difference is observed in the switching times for the same $V_s$, and two different $V_e$ voltages in the simulations.

It is challenging to use a system with a large variance in switching time between symbols for wireless communications. This is because the symbol duration will not be constant. During demodulation, it creates an additional chal-

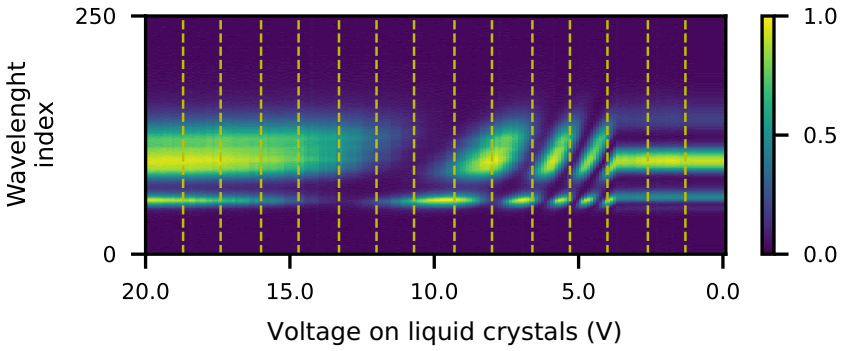


Figure 4.1: **Selection of 16 voltage levels for computation of settling time marked with yellow dashed lines.**

lenge for the receiver to demarcate the symbol boundaries of the variable length symbols. This also leads to nondeterministic packet transmission time for the same packet length in symbols.

To overcome this limitation, our approach follows two steps to define a *constant* symbol period:

- First, we measure the settling time in various regions of the spectrum in order to identify the region with the shortest switching times.
- Second, we select symbols in this *'fast-transitioning region'* found in the first step, and define the symbol period as the slowest transition among these symbols.

The supplier of our LC cells does not provide us with the specifications of all the optical properties of the pi-cells used. Hence, we are unable to use simulations to find the settling time behavior of the LCs cells. So we resort to empirical measurements to analyze the best settling times to achieve the required modulation.

### 4.1.1 Settling time measurement

If we select voltage levels that have low settling time - we will be able to switch between symbols faster during communication. To analyze the settling time behavior of the LCs, we choose sixteen points (voltage levels) spanning the spectrum, like shown in Figure 4.1. These voltage levels are spaced equidistantly over the whole spectrum. We then observe the optical transitions between every voltage pair for a duration of 50 ms. The objective of this experiment is to determine the *fastest* operating region of the spectrum. We are not selecting any symbols yet.

Figure 4.2 depicts an example of our method to calculate the settling time. A transition between the 3rd (4 V) and 2nd (2.7 V) voltage levels is used for this example. The left side plot shows the optical change in the spectrum, and the right side plot shows the calculation of settling time.

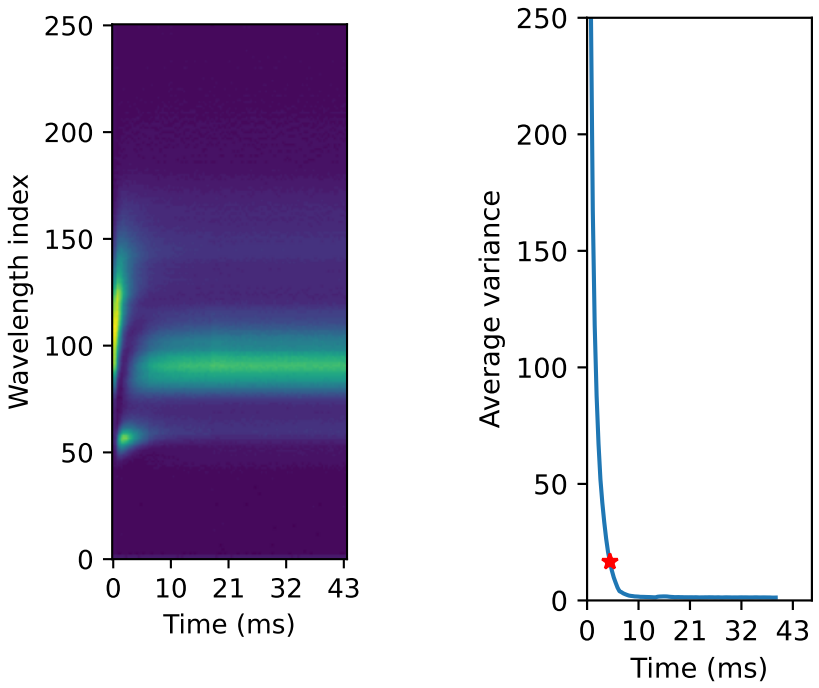


(a) Transition observed

(b) Variance with Time

Figure 4.2: **Example of a symbol transition and corresponding settling-time calculation.**

To calculate the settling time, a moving window is run along the horizontal axis, and the variance within the window is calculated for each wavelength (vertical axis). Then, we average the variance across all wavelengths for each vertical point. The settling time is defined as the point when the variance decays below a predetermined threshold (set to 20). Notice that the spectrum remains stable after the initial transition. Following these steps, we generate the settling time matrix shown in Figure 4.3, where the vertical axis represents the start voltage $V_s$ and the horizontal axis represents the end voltage $V_e$, from the voltage levels shown in Figure 4.1.

### 4.1.2 Analysis of the settling time matrix

From the matrix seen in Figure 4.3, we can conclude that:

1. The settling time matrix is asymmetric.

2. There is a sharp decrease in settling time when $V_e$ is above the fourth voltage level (5.3V).

3. The switches between the higher voltage levels are faster.

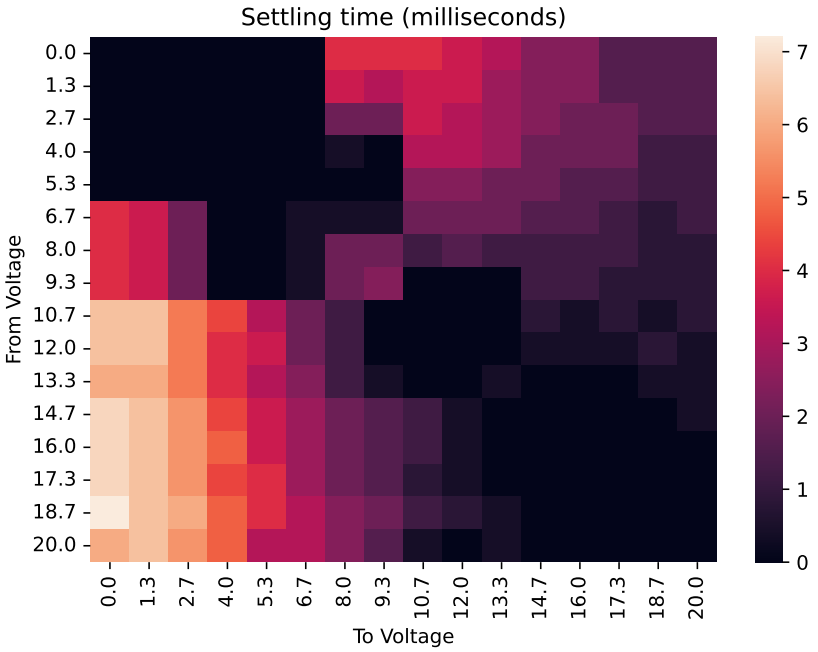


Figure 4.3: **Settling time heatmap.**

The asymmetry is explained by the fact that when a rising pulse is applied on the cells, i.e. $V_e > V_s$, the liquid crystal changes under the influence of an electric field, whereas when $V_e < V_s$, the molecules rely on inertial forces to realign themselves. As the force applied by the electrical field is much stronger than the inertial forces, the switches with rising voltages yield faster transitions.

The decrease in settling time when $V_e$ crosses the fourth voltage is explained by Chen et. al. who show that the relaxation times start to increase in this region around the critical voltage $V_c$ [10]. Although the switching times in the upper-right corner of the matrix are also quick, they all output a similar spectrum. This can be seen in the characteristics in Figure 3.10 where the spectrum appears constant below the critical voltage level.

The most important takeaway from this analysis is that the fastest transitions occur in the dark region of the lower right-hand corner. This region use higher voltages, and all the transitions take around 2.5 ms in both directions. Utilizing the entire matrix would entail considering settling times as high as 8 ms, reducing the data rate by a factor of $\times 3.2$. However, using this faster region has the disadvantage of narrowing the operating region. This reduces the signal-to-interference-and-noise ratio (SINR) as the distance between the symbols chosen is smaller.

Given that the capacity of a channel grows *linearly* with bandwidth (shorter symbol period) but only *logarithmically* with the SNR –as stated by the well-known Shannon equation–, our design prioritizes bandwidth over SNR, and thus, we choose a *few fast symbols* instead of selecting *many slow symbols*. Next, we show how symbols are actually selected and modulated.

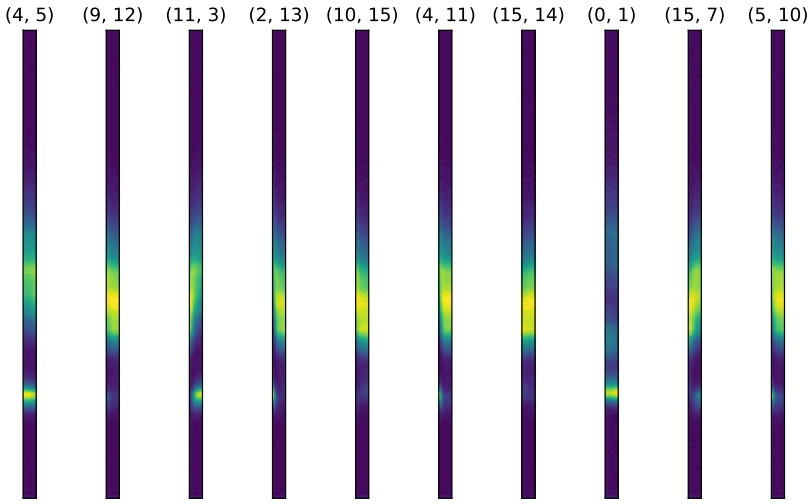


Figure 4.4: **Examples of optical transitions in the light spectrum when using a stack of 4 pi-cells.**

## 4.2 Symbol Selection & Modulation

So far, we have considered the operation spectrum of the LCs and extended their optical characteristics by stacking them. We also looked into the settling time characteristics to find the fastest region of operation. Now we take a look at the challenges faced when actually selecting symbols for our communication link.

### 4.2.1 Borders vs. Transitions

Recalling from chapter 3, the time-response of LCs displays a capacitive effect with an exponential trend similar to the charging and discharging voltage curves observed using a capacitor. When the voltage on the LCs is switched, it affects the light spectrum, leading to a *transition* in the spectrogram. The state of the spectrum when the transition is complete is called a border (corresponding to a specific voltage level). A few examples of optical transitions between symbols can be seen in Figure 4.4, where we use the convention ($n_s$ , $n_e$) to show the transition between a start ($n_s$) and an end ($n_e$) symbol.

An intuitive approach to select symbols would be to use only the borders, such as those marked by yellow lines shown in Figure 4.1. However, we find that using this approach can lead to inter-symbol interference. In our analysis, the settling time was found by observing the average variance of the spectrum and waiting for it to fall below a certain threshold (the red star in Figure 4.2). This method introduces some uncertainty in the final state of the LCs after a voltage switch. Because the LCs do not completely settle to a specific state, the inaccuracy accumulates into a spectrum drift. After the first few symbols are transmitted, the system stops reaching the desired (voltage) spectrum due to this spectrum drift. This may lead to demodulation errors. The design choice of using a threshold for settling time is intentional - to avoid lengthy waiting

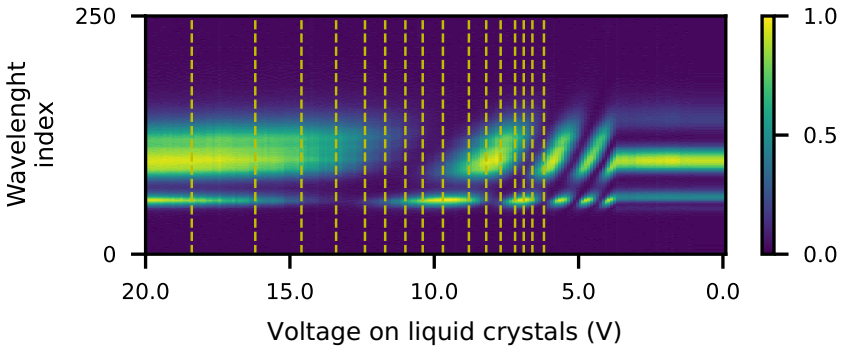


Figure 4.5: **Selected symbols based on K-means clustering.**

times, and this problem arises due to the inherent characteristics of operating LCs.

To address this issue we make use of the capacitance effect of LC cells. When the voltage is switched there is a rapid initial change followed by a slow change to settle at the steady state. By oversampling, we can use all the information captured by the transition between two borders, which includes the distinctive signature of the (dis)charge curve. When discussing demodulation in chapter 5, we will consider several ML approaches and show that transitions can also be used for effective clock synchronization.

During the evaluation, we compare both approaches to show the strength of using transitions instead of the more intuitive borders.

### 4.2.2 Selection of borders

The prior subsection argues that using transitions is more reliable than using borders, but we still need to determine which voltage levels (borders) we will use.

We place symbols at equidistant voltage levels because the spectrum in Figure 4.1 shows a pseudo-linear relation between the intensity and applied voltage. Given that in a linear function, the inter-symbol distance is maximized with an equidistant spacing, this approach should provide a competitive symbol selection. We use the voltage levels in the fast transitional region identified from the settling time analysis in subsection 4.1.2.

Another possible approach would be to use a clustering method. K-means is an unsupervised learning method, and is already optimized to minimize intra-cluster distance and maximize inter-cluster distance. We use k-means clustering to divide the spectrum into k clusters (symbols), which we expect would increase the SINR of the selected symbols (clusters). The cluster centers are selected as the borders, shown in Figure 4.5. However, when we tested this approach the results were poor. This is because the light spectrum varies with light source and intensity, and the selection by clustering would have to be re-computed after each change. As the pseudo-linear behavior is visible in all spectra, we continue using only the equidistant approach henceforth.

# Chapter 5

# Demodulation

In this section, we first look at the core of the demodulation process - the spectrogram measured at the receiver. We then begin the demodulation steps with a novel method to recover the clock (i.e. identify the location of symbols and packets) from the spectrogram. Due to challenges explained later (section 5.3), we opt to use machine learning for demodulation. As our link will work in an embedded application, we need to reduce the size of the machine learning models to utilize memory efficiently. To solve this, we explain our approach to recognize and use only the most relevant features in the spectrogram. We propose using machine learning algorithms to train online and classify the symbols. In the final part of this section, we explain how the machine learning models will recognize the symbols from the spectrogram snippets.

## 5.1 Received spectrograms

At the receiver, a spectrometer captures the wavelengths of the light coming from the transmitter. A sample signal is shown at the top of Figure 5.1. The horizontal axis shows the time samples, and the vertical axis shows each wavelength. We can see that different patterns are generated when the voltage applied on the LC stack changes. The receiver captures the spectrogram as a $w \times m$ matrix where $w$ is the number of wavelengths captured by the receiver, and $m$ is the number of samples captured.

## 5.2 Clock recovery & symbol extraction

The communication link requires extracting the symbols from the spectrograms. To achieve this goal, we perform two steps: clock recovery and the actual symbol extraction as described below.

### 5.2.1 Clock recovery

To identify the symbols' period, we design a preamble that causes abrupt changes in the spectrogram (so the preamble can be easily detected). The packets' preamble is designed to serve two purposes:

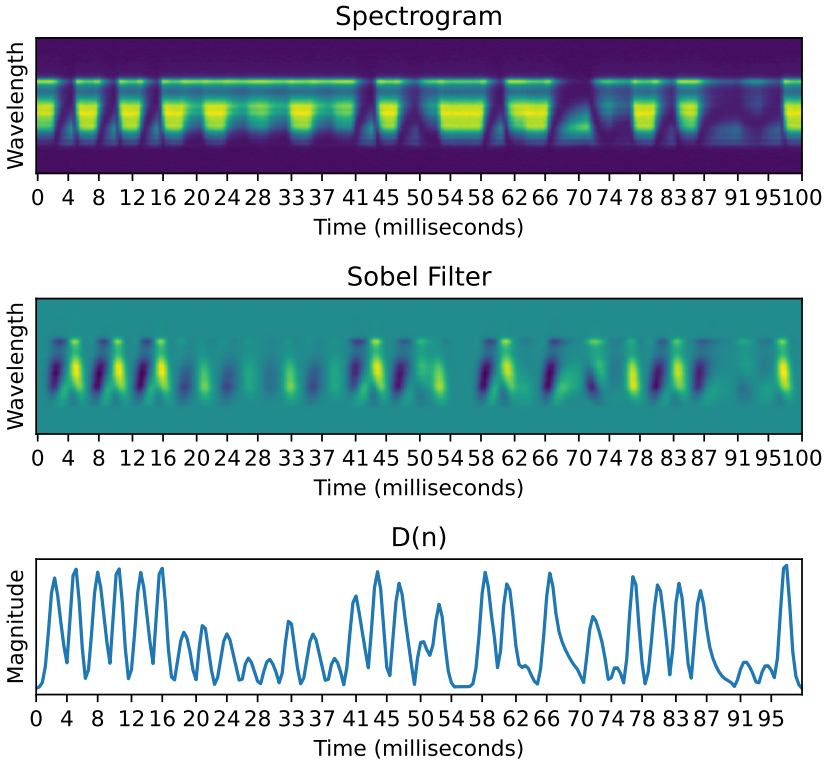


Figure 5.1: **Spectrogram with Sobel filter and D(n) of an example packet consisting of a preamble (first six symbols) and a payload (remaining symbols).**

1. Recovering the transmitter's clock

2. Marking the start of the payload

To detect the changes in the preamble, we consider the capacitance model discussed in subsection 4.2.1: when the voltage on the pi-cells switch from one symbol to another, the spectrogram changes with the highest gradient at the beginning, and the rate of change decreases as the LC reaches its final state.

To reveal the beginning of symbols, we run a Sobel filter along the horizontal axis of a spectrogram. The Sobel filter is a 1-d derivative in image processing used to measure gradients. The output of this filter is a matrix of the same size as the original image, as shown in the middle of Figure 5.1. By summing this matrix along each column we get the curve D(n) shown at the bottom of Figure 5.1. The peaks in D(n) denote the times when the voltage on the LCs is switched, i.e. when the capacitance model exhibits the fastest change. To maximize the likelihood of detecting the peaks in the preamble, we use the two most-extreme symbols in the constellation. The transmitter sends six consecutive transitions between those two extreme symbols, as shown at the bottom of Figure 5.1.

### 5.2.2 Symbol extraction

In theory, every transition between symbols should be detected in the Sobel plot. In practice, not all the beginnings of symbols generate a clear peak. This occurs mainly when similar or very close symbols are sent consecutively. Such an example is shown Figure 5.1 at around 54 ms where the payload contains two identical symbols back-to-back.

In this case, we have to estimate the beginning of the symbols based on the clock information obtained in the previous step. Whenever the distance between two peaks in the Sobel plot is greater than one clock cycle, we divide that period into smaller components equal to the clock duration.

To test the validity of this method, we use a "helper wire" between the transmitter and the receiver, signaling the start of packets and symbols. The estimated symbol borders turned out to be exactly the same as the ground truth. In Figure 5.2, we show the results of our peak finding approach. The red (dashed) lines mark the beginning of a packet, the white lines mark the symbol transitions detected by the Sobel plot (i.e. clear peaks), and the yellow lines mark the transitions detected through the use of the inferred clock (i.e. unclear peaks).

An important consideration in our approach is to minimize drift effects (accumulation of errors due to inexact measurements of the symbol period). If the transmitter's frequency and the receiver's sampling rate are not defined well, the number of samples per symbol varies. For example, the matrix of one symbol may have $c$ columns, and the next symbol may have $c + 1$ columns. These variations may seem small, but they can cause severe detrimental effects on the machine learning process.

To avoid this problem, we make sure that the receiver captures an equal number of samples per symbol by setting the receiver's sampling rate as an *integer multiple* of the symbol clock.

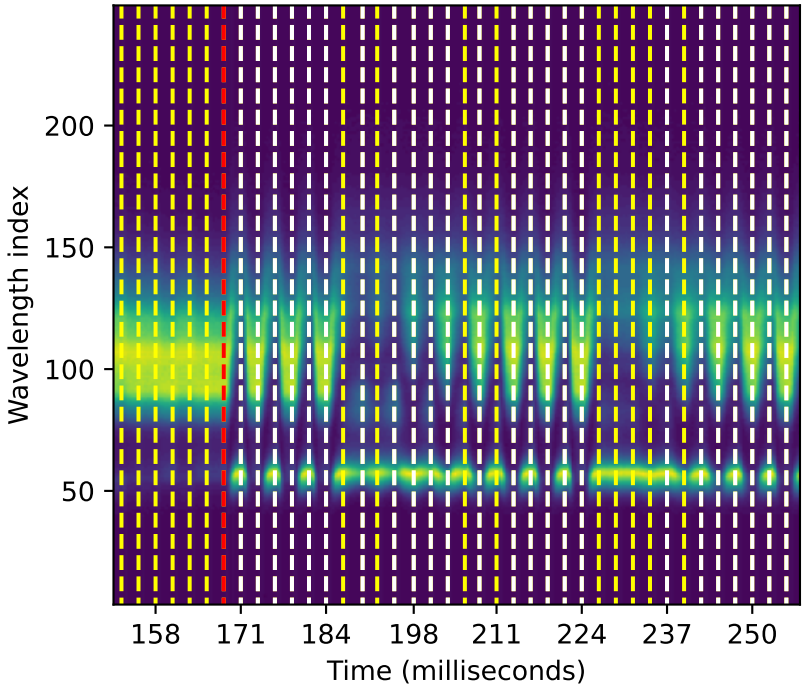


Figure 5.2: **Annotated spectrogram showing transitions between symbols (red = start of the preamble; white = start of symbol; yellow = inferred start).**

## 5.3 Identification of symbols

So far, we have shown how the clock can be recovered and the symbols extracted as fragments from the spectrogram. Each symbol shows the transition of the spectrum after the voltage has been switched on the LC stack. We need to be able to classify these snippets extracted from the spectrogram to recover the symbols that were transmitted.

The main challenge here is that the spectra emitted from various light sources differ from each other, as illustrated in Figure 5.3, and also have varying intensities. Generalization of this highly varying spectral behavior is challenging and entails a flexible solution that can adapt to new scenarios fast. That is why we propose using simple machine learning algorithms to learn the spectral properties of the symbols online, and classify the symbols extracted from the data message.

Before that, we need to reduce the large number of input pixels to suit an embedded application in the final solution. In the next step, we identify the important features from the spectrogram snippets to reduce the size of the machine learning models.

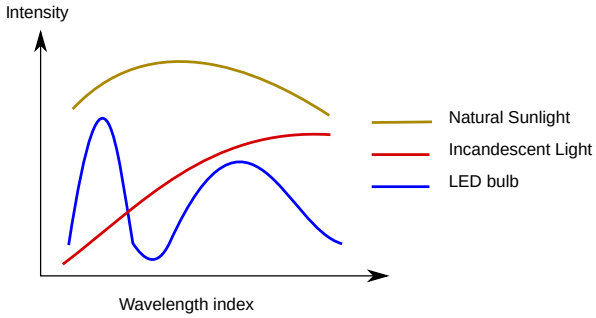


Figure 5.3: **Typical spectral output for various light sources.**

## 5.4 Feature extraction

With the borders found in the previous step, the spectrogram is split into smaller matrices (slices) for each symbol. The size of each matrix is $w \times n$, where $w = 250$ (number of wavelengths) and $n = 7$ (number of samples).

The number of samples follows from the settling time and sampling rate of the spectrometer, so it cannot be changed. Some examples of "transition slices" can be seen in Figure 5.2.

The problem with these matrices is that they are big. For example, if we would like to use a neural network for classification, we would require 1750 inputs ($7 \times 250$), increasing the complexity of the overall system. To reduce this size while retaining the most important information for each symbol, we apply Principal Component Analysis (PCA).

PCA is a statistical technique commonly used for feature reduction in machine learning models [4]. PCA offers a change in perspective of the data distribution, by transforming the data's coordinate system. In the transformed data, the samples with the largest variance are aligned along the primary axis, with all other axes aligned in decreasing order of variance. The order of the contributing variance is determined by analysis of the eigenvalues of the variance-covariance matrix of the normalized dataset. By discarding the components with low variance, most information can be preserved using significantly fewer parameters. Prior works have also used PCA to reduce the features in an audio spectrogram in phonetics identification for human speech [24].

PCA dramatically reduces the dimension of the original dataset[1]. Figure 5.4 depicts the information captured by the most relevant components. We can observe that the fifteen most relevant dimensions capture most of the information, reducing the input size by more than x100. To be on the conservative side, in our implementation, we use the 128 most important components, which capture 99.56% of the original variance in the data. Our approach reduces the size only by a factor of x14, but the input is already small enough to run the classification algorithm in a resource-constrained embedded system.

[1]The PCA implementation is obtained from scikit-learn [23].

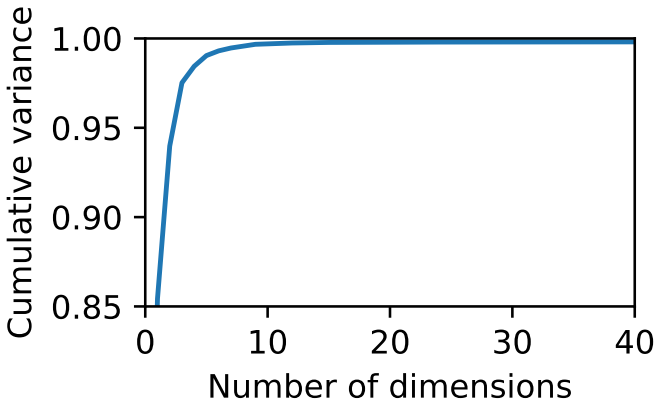


Figure 5.4: **Cumulative variance preserved with the number of PCA dimensions.**

## 5.5 Classification

There are various machine learning methods that can be used to classify the features obtained from the PCA results.

In chapter 6, we compare the performance of four machine learning models:

**Support Vector Machine (SVM)** SVM maximizes the margin between the different classes [12]. Our implementation uses a radial bias function kernel to draw a non-linear boundary. It uses a One vs. One strategy to predict the multi-class labels of the transitions.

**K-st Nearest Neighbors (K-NN)** K-NN works by making a decision after considering the majority of the k closest neighbors [16]. We utilize Euclidean distances, and based on the results of chapter 6, we find k=5 neighbors to be optimal.

**Random Forest Classifier (RF)** Random Forests use an ensemble of decision trees to make a prediction [6]. A decision tree makes successive partitions of the training data based on Gini impurity scores, attempting to maximize the separation of the different classes. In our implementation, we use 100 trees. We estimate this number of trees to be a sufficiently large ensemble for this data.

**Neural Network (NN)** A simple neural network of one input layer, two hidden layers, and one output layer is used. The model is trained for 500 epochs with a batch size of 1024. We performed a grid search to arrive at these values.

We use an implementation from scikit-learn [23, 13] for the SVM, K-NN and RF classifiers, and an implementation from Keras [11] for the Neural Network. In chapter 6, we use training packets (see below) to obtain the features of each symbol and data packets to measure the quality of the link in terms of its Bit-Error-Rate (BER). An overview of the entire communication process can be seen in Figure 5.5.

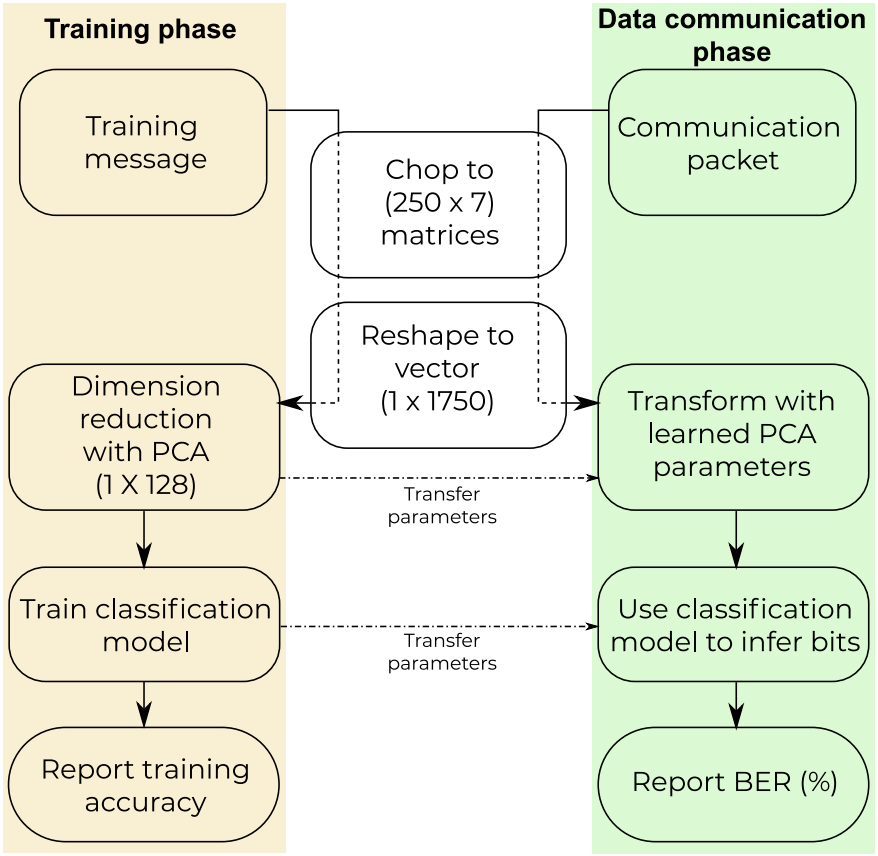


Figure 5.5: **Flowchart of training and demodulation processes.**

## 5.6 Training

Machine learning models need to be trained before they can be put to use. In our case, we need to provide them with enough data so that the model parameters for classifying the $n \times n$ transitions can be learned. In the online phase, these parameters can then be used to extract (infer) the bits from the packets sent across a live communication link. To this end, we have defined a training packet that simply includes $n^2 + 1$ symbols as the payload[2]. This training packet will then be sent repeatedly across to account for any noise and external factors impacting the communication link. Exactly how much training data needs to be collected is not clear a priori; the classification accuracy depends not only on the noise but also on the ML algorithm, and will be studied in chapter 6.

[2]Instead of concatenating $n^2$ pairs of symbols, they can be chained such that the end symbol of one transition serves as the start of the next, requiring only one extra symbol.

# Chapter 6

# Evaluation and Analysis

In this section, we evaluate the performance of our system and measure the bit error rate (BER) in various scenarios considering different number of symbols, distances, light sources, and ambient lighting conditions. First, we evaluate the method proposed in subsection 4.2.1, where we claim that using transitions between symbols to train our model is a better option compared to using the symbols themselves, and we show that the former method outperforms the latter. Then, we expose our system to different working conditions. And in the last part, we address the training cost of the machine learning models used for classification.

## 6.1 Borders versus transitions

During the demodulation, we use the entire transition between the two voltages (symbols) for the classification task. However, this increases the required training data quadratically. Due to this trade-off, we need to evaluate both methods to verify the advantage of using transitions. When using transitions, the minimum symbol clock that results in acceptable BERs is 2.6 ms. On the contrary, when using borders (symbols) only, we have to wait long enough for a transition to settle, which turns out to be 3.6 ms.

*Basic setup*: To have a controlled environment, we set the experiments in a dark room with a light source placed directly behind the LCs. In this way, we minimize errors due to external sources and capture only the performance of the modulating technique.

With this basic setup, we set the transmitter and receiver at a 20 cm distance and transmit with a constellation of $n = 8$ symbols, so 3 bits per symbol. The size of each packet is 78 symbols (0.2 seconds for each packet including the preamble and the 72 transitions due to how 8 symbols are arranged). The sequence of transitions in the training packets is known, while data packets contain random sequences. For all the experiments done in this section (with different ranges, light sources and light intensities), we transmit 60 packets for training and 60 for data.

Figure 6.1 shows the results of the borders vs. transitions experiment. Comparing figures with different symbol durations shows that the performance of the method using symbols (borders) degrades significantly when the symbol period

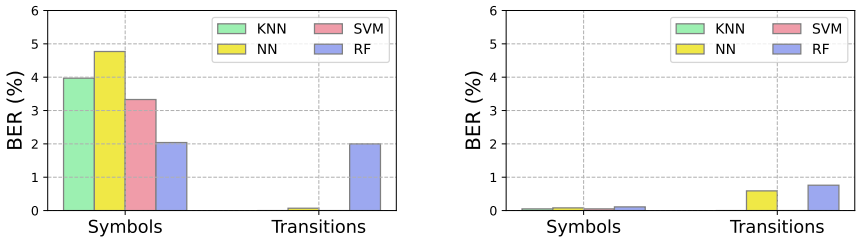


(a) Symbol clock 2.6 ms

(b) Symbol clock 3.4 ms

Figure 6.1: **Comparison of BERs between using transitions and borders in the training and demodulation process.**

decreases to 2.6 ms. Hence, despite the heavier computational requirement, we use transitions for our (de)modulation systems. In chapter 8, we discuss some possible solutions to reduce the training overhead.

## 6.2 Comparison of ML algorithms

Now, we will compare the performance of the machine learning models introduced in chapter 5: Support Vector Machine (SVM), K Nearest Neighbour (K-NN), Neural Network (NN), and Random Forest (RF). For this purpose, we use the same *basic setup* as the prior section, but we test three different ranges (20, 40 and 80 cm). We also consider two settings for the link's data rate. One setting with 8 symbols, leading to a data rate of 1.1 kbps, and the other setting with 16 symbols, leading to a data rate of 1.5 kbps. The packet with $n = 8$ symbols is the same as in the prior experiment. The packet with $n = 16$ symbols contains 278 bytes including the preamble and 272 transitions (0.73 seconds of transmission delay per packet). Following the analysis of section 6.1, the symbol period is always kept at 2.6 ms, which is the shortest possible period as a result of the inherent settling time of LCs.

The results comparing a lower data rate with a higher data rate is shown in Figure 6.2. Observe that for the low data rate setting (8 symbols), all the machine learning methods perform well, except for RF. For the higher data rate, however, only K-NN and NN have a good performance. This occurs because SVM has a hard time defining clear boundaries between the different high-dimensional clusters. Due to this performance, in the next sections we only use K-NN and NN for the demodulation process. To have a clearer look at the results of NN and K-NN, we plot the BER for these algorithms in Figure 6.3. It can be seen that there is less than 1% BER for 1.1 kbps, and the BER reaches 6% for higher speeds.

## 6.3 Different light sources

With the *basic setup*, the light source is placed close to the LC to minimize external sources of noise. In the next experiments, we consider different light sources: a regular light bulb placed a few meters from the transmitter (as shown

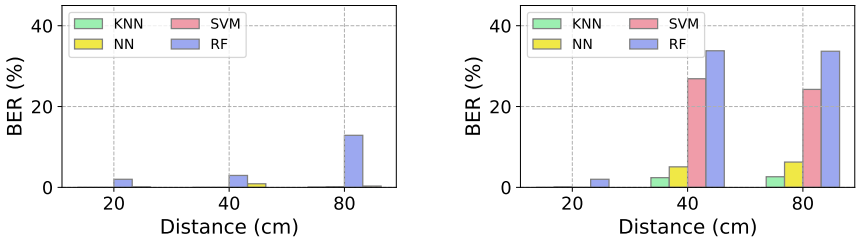


(a) Low data rate: 8 symbols

(b) High data rate: 16 symbols

Figure 6.2: **Comparison of 4 ML models: K-NN, NN , SVM , RF. The comparison is done in two different scenarios.**

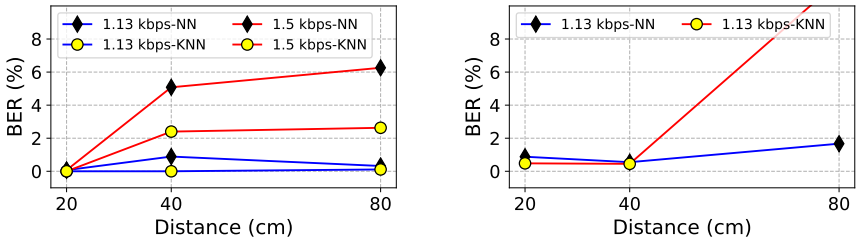


(a) Using flashlight 1.5 kLux

(b) Using light bulb 490 Lux

Figure 6.3: **Experimental results of BER with a flashlight and standard light bulb as illumination sources**

in Figure 6.6), light coming from a sunlight emulator (a complex array of LEDs that emulate the spectrum of the sun) and real sunlight. For these experiments we only test the configuration with 8 symbols at 1.1kbps. As depicted in Figure 6.3, when NN is used with the light bulb setup, the BER stays under 1 % for short distances, and under 2 % for 80 cm, however, the results show a significantly higher BER when K-NN is used. When we test the system with the sunlight emulator we get a link below 1% BER at 40 cm, and for real sunlight a BER around 2%. Beyond 40 cm, the BER increases rapidly with both, the sunlight emulator and real sunlight. This short range is due to the interference created by multiple shadows, similar to umbra and penumbra phenomena. We hypothesize that if, similar to the setup used in [14], we would place a mirror at the transmitter (to direct sunlight in a specific direction), and a well-calibrated lens at the receiver (to create a narrow field-of-view towards the transmitter), the range can be increased.

## 6.4 Variation in light intensity

In all previous experiments, the light intensity is kept constant during the training and demodulating phases. An important question is to assess the effect of varying light intensities on the BER. When using ambient light from light bulbs,

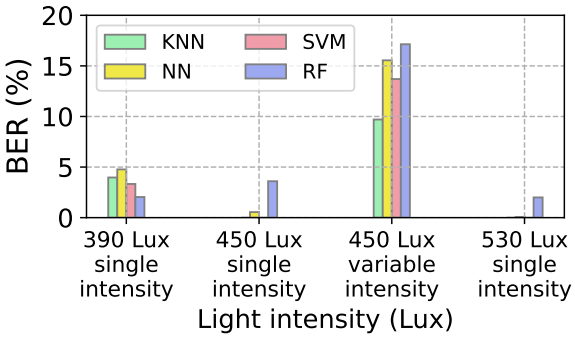


Figure 6.4: **Experimental results with varying light intensity using a flashlight, 20cm**

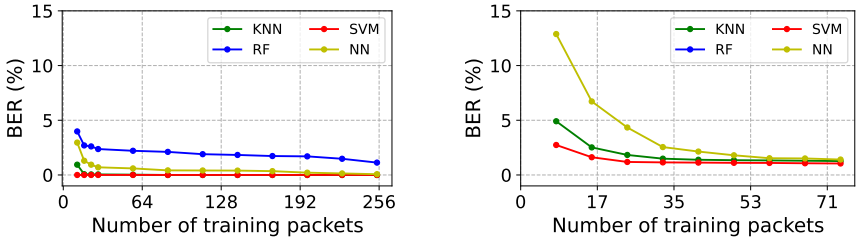


(a) 1.1 kbps

(b) 1.5 kbps

Figure 6.5: **Comparison of the amount of data required to train each ML model. The experiments are done at low and high speeds.**

we can assume that the intensity does not change significantly, so both the training and communication phases are carried out using a single light intensity. However, the assumption does not hold true in all scenarios. Under varying lighting conditions, one hypothesis is that it might be sufficient to train our model using the highest and the lowest intensities, and use the trained model on any intensity level in between. This is based on the fact that in different intensities, the spectrum *pattern* is preserved, and it is only scaled up or down in *intensity*. To test this, we collect data for 3 different intensity levels of an LED flashlight: 390, 450, and 530 Lux. Then, we train the ML models on the lowest and the highest intensities, and test it using medium intensities. To have a reference point, we also train and demodulate on each intensity level, as we did in previous experiments. The results of the experiment at 20 centimeters using the *basic setup* are shown in Figure 6.4. In this plot, the "single intensity" labels show the BER when a model is trained and tested with the same intensity, and the "variable intensity" label shows the BER when the mid-level intensity is demodulated using the ML models that are trained with low and high intensities. This figure shows that the rise in BER of the middle intensities is significant, and surpasses the requirements for a robust communication system. This implies that the system needs to be trained for different intensity

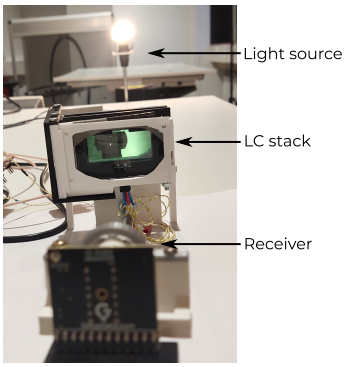


Figure 6.6: **An example of the setup for evaluation with light bulb.**

| **Training time for BER <2%** | | | | |
|---|---|---|---|---|
| **Data rate** | **Model** | **SVM** | **K-NN** | **NN** |
| 1.1 kbps | Packets required | 12 | 12 | 15 |
| | Time required (s) | 2.4 | 2.4 | 3.0 |
| 1.5 kbps | Packets required | 14 | 23 | 45 |
| | Time required (s) | 10.4 | 16.8 | 33.0 |

levels. In the next part, we analyze the cost of training a model.

## 6.5 Training overhead

Due to the overhead of the training process, and the need for retraining (as a result of the previous section) it is important to identify the minimum number of training packets required to achieve a low BER during the demodulation process. The effect of the amount of training data on the BER for each classification model can be seen in Figure 6.5. This experiment uses the data rate of 1.5 kbps, at a distance of 20 cm with the *basic setup*. We observe that the convergence time varies for each model: SVM being the fastest followed by K-NN and NN, but SVM only performs well for the basic setup. The number of packets and training time required to achieve a BER of less than 2% is shown in the table above. To put these values in context, consider a scenario where sunlight is used as a carrier, and new training packets have to be sent every 20 minutes to cope with the changes in light intensity (depending on the geographic location). Such a scenario would lead to devoting ≈1-2% of the time to training. When choosing 8 symbols (1.13 kbps), the training time would be less than one-quarter of that period.

# Chapter 7

# Conclusions

In this thesis, we established the working of spectrum-aware passive VLC, with demonstrations of feasible modulation and demodulation schemes and a working prototype. To the best of our knowledge, this is the first work to exploit the visible light spectrum for passive communication and offers a new perspective for future work in the field.

We build upon work done by Chromalux [14] to broaden the path difference of LCs by stacking, and operate them in their transient region to modify the light spectrum. We introduce the use of a spectrometer as a receiver, and overcome major hurdles to identify and distinguish the individual symbols. Our novel approach using signal processing, image processing, and machine learning allows us to surpass basic intensity modulation. The analysis of the dynamic behavior of stacked pi-cells as the transmitter is a key contribution to further studies in passive VLC using off-the-shelf LCs.

Our work achieves a higher datarate of 1.5 kbps when compared to other single pixel-transmitters, which reach a maximum datarate of around 1 kbps [21, 32, 7, 14]. In passive VLC, only RetroTurbo performs better by using a large multi-pixel array of 64 LCs for a datarate of 8 kbps [33].

Despite improving channel capacity by 1.5x, it must be noted that our system uses a much more complex receiver, and works in very selected conditions. We only lay the first stone in spectrum-aware passive VLC, and several improvements discussed in chapter 8 are possible.

Overall, this work sheds some light on the methods of controlling light's wavelengths, and introduces a novel alternative to the passive VLC community, paving the way towards a more efficient use of the ultra-wide bandwidth of visible light spectrum with available off-the-shelf devices.

# Chapter 8

# Future Work

Having established the working of spectrum-aware passive VLC, we explore the different avenues for future work in the field. While our approach changes the mindset to make modulation schemes spectrum-aware - our solution is still limited. We expect that the implementation of ideas in this chapter will improve the channel capacity and reliability of our work significantly.

## 8.1 Sub-band modulation

This work uses multiple LCs stacked together to create richer and more diverse spectra. All the light from the ambient source is manipulated together. However, independent modulation at multiple wavelength bands is also possible. This sub-band modulation technique can extend the observable spectra and subsequently increase the channel capacity.

Ambient light can be spilt into separate bands of wavelengths using dichroic filters. The different wavelength bands created by these filters can be modulated independently by using multiple LC stacks. Thus, a MISO (multiple-input and single-output) link can be created. Although this will require a significantly more complex setup - it can be expected to outperform the solution presented in this thesis.

## 8.2 Embedded hardware

Passive VLC is mostly envisioned to be used in low-power applications for IoT. This thesis establishes the proof-of-concept for spectrum-aware passive VLC, with most of the processing and analysis being done offline using a PC. During the development phase, the setup was complex as hardware choices were yet being explored.

In the next steps, the spectrometer can be integrated into a custom circuit with a micro-controller running the demodulation steps in real-time. This will reduce the hardware's size and complexity, making it suitable for mobile applications.

At the transmitter side, we still do not use the full voltage range that the pi-cells can tolerate due to the limitations of the signal generator. Operating at higher voltages has some benefits like faster switching times and hence has the

potential to increase the datarate of our system. However, these voltages will lead to larger power consumption, which is unsuitable for embedded applications. Nevertheless, the potential to extend the optical spectrum can significantly reduce the BER as the symbols can be spaced further away.

## 8.3 Material science improvements

Most of the work in Passive VLC, including our own, use readily available LCs off-the-shelf for modulation. As LCs are typically only used as optical shutters to block/allow light passing through, there is only a limited understanding of the optical characteristics in the transient region. Many necessary specifications of the optical properties of the LCs are also not easily available from suppliers. In our opinion, if suppliers work closely with research in passive VLC, dedicated LC cells with required optical properties like broader path difference can improve performance. As dedicated hardware will have lesser attenuation of the signal, it will improve performance.

## 8.4 Channel estimation

A huge limitation in this work is scalability. The time required for channel estimation grows quadratically with the number of symbols selected. This is because for any $n$ symbols, we need to send the transitions between all $n^2$ possible pairs for training. However, with an in-depth optical understanding we could use simulations to predict the transitional behavior. The training data collection phase could be eliminated in this way. More number of symbols could be selected, increasing the channel capacity.

# Bibliography


[1] Liquid crystal technologies. http://liquidcrystaltechnologies.com/, 2016. Accessed: 2022-05-12.

[2] Pi-cell behavior. http://liquidcrystaltechnologies.com/tech_support/Pi_Cell.htm, 2016. Accessed: 2022-08-17.

[3] Benchtop spectroscope. https://www.patonhawksley.com/product-page/benchtop-spectroscope, 2022.

[4] Hervé Abdi and Lynne J Williams. Principal component analysis. *Wiley interdisciplinary reviews: computational statistics*, 2(4):433–459, 2010.

[5] Chanda Bhabatosh et al. *Digital image processing and analysis*. PHI Learning Pvt. Ltd., 1977.

[6] Gérard Biau and Erwan Scornet. A random forest guided tour. *Test*, 25(2):197–227, 2016.

[7] Rens Bloom, Marco Zúñiga Zamalloa, and Chaitra Pai. Luxlink: creating a wireless link from ambient light. In *Proceedings of the 17th Conference on Embedded Networked Sensor Systems*, pages 166–178, 2019.

[8] Chun-Ling Chan, Hsin-Mu Tsai, and Kate Ching-Ju Lin. Poli: Long-range visible light communications using polarized light intensity modulation. In *Proceedings of the 15th Annual International Conference on Mobile Systems, Applications, and Services*, MobiSys '17, pages 109–120, New York, NY, USA, 2017. ACM.

[9] Shu-Hsia Chen and Chiu-Lien Yang. Dynamics of twisted nematic liquid crystal pi-cells. *Applied physics letters*, 80(20):3721–3723, 2002.

[10] Hongfei Cheng and Hongjin Gao. Dynamic simulation of pi-cell liquid crystal displays. *Liquid Crystals*, 28(9):1337–1341, 2001.

[11] François Chollet et al. Keras. https://keras.io, 2015.

[12] Corinna Cortes and Vladimir Vapnik. Support-vector networks. *Machine learning*, 20(3):273–297, 1995.

[13] Aurélien Géron. *Hands-on machine learning with Scikit-Learn, Keras, and TensorFlow: Concepts, tools, and techniques to build intelligent systems.* " O'Reilly Media, Inc.", 2019.

[14] Seyed Keyarash Ghiasi, Marco A Zúñiga Zamalloa, and Koen Langendoen. A principled design for passive light communication. In *Proceedings of the 27th Annual International Conference on Mobile Computing and Networking*, New York, NY, USA, September 2021. ACM.

[15] Ian Goodfellow, Yoshua Bengio, and Aaron Courville. *Deep Learning*. MIT Press, 2016. `http://www.deeplearningbook.org`.

[16] Gongde Guo, Hui Wang, David Bell, Yaxin Bi, and Kieran Greer. Knn model-based approach in classification. In Robert Meersman, Zahir Tari, and Douglas C. Schmidt, editors, *On The Move to Meaningful Internet Systems 2003: CoopIS, DOA, and ODBASE*, pages 986–996, Berlin, Heidelberg, 2003. Springer Berlin Heidelberg.

[17] Mohamed Ibrahim, Viet Nguyen, Siddharth Rupavatharam, A. Jawahar, Marco Gruteser, and Richard Howard. Visible light based activity sensing using ceiling photosensors. pages 43–48, 10 2016.

[18] M. I. Jordan and T. M. Mitchell. Machine learning: Trends, perspectives, and prospects. *Science*, 349(6245):255–260, 2015.

[19] R. Kanaris-Sotiriou. Bloss, F.D. Optical Crystallography.: Mineralogical Society of America Monograph Series, Publication #5, 1999. 239 pp. Price U.S.
32.00; *U.S.*
24.000 for MSA members. ISBN 0-939950-49-9. *Mineralogical Magazine*, 64(4):777–778, 08 2000.

[20] Brian E.D Kingsbury, Nelson Morgan, and Steven Greenberg. Robust speech recognition using the modulation spectrogram. *Speech Communication*, 25(1):117–132, 1998.

[21] Jiangtao Li*, et al.* Retro-vlc: Enabling battery-free duplex visible light communication for mobile and iot applications. In *HotMobile*, 2015.

[22] Shimwe Dominique Niyonambaza, Elodie Boisselier, Mounir Boukadoum, and Amine Miled. A compact visible light spectrometer for molecular detection with spherical gold nanoparticles. In *2019 41st Annual International Conference of the IEEE Engineering in Medicine and Biology Society (EMBC)*, pages 1058–1061, 2019.

[23] F. Pedregosa, G. Varoquaux, A. Gramfort, V. Michel, B. Thirion, O. Grisel, M. Blondel, P. Prettenhofer, R. Weiss, V. Dubourg, J. Vanderplas, A. Passos, D. Cournapeau, M. Brucher, M. Perrot, and E. Duchesnay. Scikit-learn: Machine learning in Python. *Journal of Machine Learning Research*, 12:2825–2830, 2011.

[24] Ben Pinkowski. Principal component analysis of speech spectrogram images. *Pattern Recognition*, 30(5):777–787, 1997.

[25] Sihua Shao, Abdallah Khreishah, and Hany Elgala. Pixelated vlc-backscattering for self-charging indoor iot devices. *IEEE Photonics Technology Letters*, 29(2):177–180, 2017.

[26] Bjørn Sørensen. A revised michel-lévy interference colour chart based on first-principles calculations. *European Journal of Mineralogy*, 1, 02 2013.

[27] Zhao Tian, Charles J Carver, Qijia Shao, Monika Roznere, Alberto Quattrini Li, and Xia Zhou. Polartag: Invisible data with light polarization. In *Proceedings of the 21st International Workshop on Mobile Computing Systems and Applications*, pages 74–79, 2020.

[28] Zhao Tian, Yu-Lin Wei, Wei-Nin Chang, Xi Xiong, Changxi Zheng, Hsin-Mu Tsai, Kate Ching-Ju Lin, and Xia Zhou. Augmenting indoor inertial tracking with polarized light. In *Proceedings of the 16th Annual International Conference on Mobile Systems, Applications, and Services*, MobiSys '18, pages 362–375, New York, NY, USA, 2018. ACM.

[29] Jesse R. Vanderveen, Brian Martin, and Kristopher J. Ooms. Developing tools for undergraduate spectroscopy: An inexpensive visible light spectrometer. *Journal of Chemical Education*, 90(7):894–899, 2013.

[30] Marian Verhelst and Bert Moons. Embedded deep neural network processing: Algorithmic and processor techniques bring deep learning to iot and edge devices. *IEEE Solid-State Circuits Magazine*, 9(4):55–65, 2017.

[31] Avery Wang. An industrial strength audio search algorithm. 01 2003.

[32] Purui Wang, Lilei Feng, Guojun Chen, Chenren Xu, Yue Wu, Kenuo Xu, Guobin Shen, Kuntai Du, Gang Huang, and Xuanzhe Liu. Renovating road signs for infrastructure-to-vehicle networking: a visible light backscatter communication and networking approach. In *Proceedings of the 26th Annual International Conference on Mobile Computing and Networking*, pages 1–13, 2020.

[33] Yue Wu, Purui Wang, Kenuo Xu, Lilei Feng, and Chenren Xu. Turboboosting visible light backscatter communication. In *Proceedings of the Annual conference of the ACM Special Interest Group on Data Communication on the applications, technologies, architectures, and protocols for computer communication*, pages 186–197, 2020.

[34] Xieyang Xu*, et al.* PassiveVLC: Enabling practical visible light backscatter communication for battery-free iot applications. In *MobiCom*, pages 180–192, 2017.

[35] Zhice Yang, Zeyu Wang, Jiansong Zhang, Chenyu Huang, and Qian Zhang. Wearables can afford: Light-weight indoor positioning with visible light. In *Proceedings of the 13th Annual International Conference on Mobile Systems, Applications, and Services*, MobiSys '15, pages 317–330, New York, NY, USA, 2015. ACM.

[36] Leah Ziph-Schatzberg, Thomas Bifano, Steven Cornelissen, Jason Stewart, and Zvi Bleier. Secure optical communication system utilizing deformable MEMS mirrors. In Scot S. Olivier, Thomas G. Bifano, and Joel A. Kubby, editors, *MEMS Adaptive Optics III*, volume 7209, pages 96 – 110. International Society for Optics and Photonics, SPIE, 2009.

[37] V. Zue and R. Cole. Experiments on spectrogram reading. In *ICASSP '79. IEEE International Conference on Acoustics, Speech, and Signal Processing*, volume 4, pages 116–119, 1979.

# Appendix A

# Power consumption and cost

As low power operation is a key point for passive VLC, we take a look at the costs and power consumption of our system in this section.

### Costs

The cost of the main components in the transmitter and receiver are listed below. We choose the best integrated spectrometer available for embedded applications offering sufficient resolution and accuracy. However, with some engineering effort, accurate but cheaper spectrometers can also be made using analog spectrometers [3] and high-speed image sensors.

| **List of key components** | | | |
|---|---|---|---|
| Component | Tx or Rx | count | Price per item |
| STM32 microcontroller | both | 2 | 12 euros |
| Spectrometer | Rx | 1 | 290 euros |
| Lens | Rx | 1 | 5 to 25 euros |
| Pi-cell | Tx | 4 | 15 euros |

### Transmitter's power consumption

The power consumption of the transmitter is determined primarily by the speed of operation. By modelling LCs as capacitors, we can use the following equations to calculate the power consumption:

$$P = CV^2 f$$

where C is the LC's capacitance, V is the voltage swing on the capacitor, and f is the frequency of the voltage V. Our measurements show that each pi-cell has a capacitance of about 6.7 nF. Following the modulation method explained in Section 4, a 1 kHz pulse is put on 4 pi-cells. With V peaking at 20 volts, the total power consumption is shown in the table below:

| **Transmitter's power consumption @ 1.3 kbps** | | |
|---|---|---|
| Component | Operating voltage | Power consumption |
| Pi-cells | 2 V to 20 V | 0.7 mW |

This sub-milliwatt consumption of LC cells is in agreement with the values reported by other passive VLC studies [34, 14].

**Receiver's power consumption**

In the receiver, the power consumption depends mainly on the clock frequency of the spectrometer sensor. In our case, the spectrometer is clocked with a 2.4 Mhz pulse. Following the information in the datasheet of the spectrometer, its power consumption is summarized below:

| **Receiver's power consumption** | | |
|---|---|---|
| Component | Operating voltage | Power consumption |
| Spectrometer | 5 V | 0.166 mW |
| Driving circuit | 3.3 V | 50 mW |